



Natural and Mixed Convection in Square Vented Enclosure Filled with Metal Foam

Lect. Dr. Luma Fadhil Ali

Department of Mechanical Engineering

College of Engineering

Baghdad University

E-mail: luma.fadhil@yahoo.com

ABSTRACT

Steady natural and mixed convection flow in a square vented enclosure filled with water-saturated aluminum metal foam is numerically investigated. The left vertical wall is kept at constant temperature and the remaining walls are thermally insulated. Forced convection is imposed by providing an inlet at cavity bottom surface, and a vent at the top surface. Natural convection takes place due to the temperature difference inside the enclosure. Darcy-Brinkman-Forchheimer model for fluid flow and the two-equation of the local thermal non-equilibrium model for heat flow was adopted to describe the flow characteristics within the porous cavity. Numerical results are obtained for a wide range of width of the inlet as a fraction of the height of the enclosure ($D/H = 0.1 - 0.6$), the porosity of aluminum foams ($\varepsilon = 0.91, 0.97$), Grashof numbers ($Gr = 10^4 - 3 \times 10^6$), and Reynolds number ($Re = 1 - 20$). Effects of pertinent physical parameters are performed in terms of the flow and temperature fields, as well as the average Nusselt number variations. The results show that the average Nusselt number increases with D/H and Re and decreases with the porosity increasing. The fluid temperature distribution has a little difference from the solid matrix temperature distribution.

Key words: mixed convection, square vented enclosure, thermal non-equilibrium, numerical study, metal foams, porous media.

الحمل الحر و المختلط في حيز مربع يحوي فتحات و مملوء برغوة معدنية

م.د. لى فاضل علي

قسم هندسة الميكانيك

كلية الهندسة / جامعة بغداد

الخلاصة:

يقدم البحث الحالي دراسة نظرية لأنتقال الحرارة بالحمل الطبيعي و المختلط المستقر في حيز مربع ذو فتحات مملوء برغوة معدنية من الالمنيوم مشبعة بالماء. لقد تم تثبيت درجة حرارة الجدار العمودي الايسر مع ابقاء الجدران المتبقية معزولة حراريا. ان الحمل القسري يتكون عن طريق فتحة الدخول الموجودة على السطح السفلي و فتحة التهوية المقابلة لها في السطح الاعلى. الحمل الحراري الحر يتكون نتيجة لأختلاف درجات الحرارة داخل الحيز. تم استخدام معادلة دارسي-برنكمان-فورشهيمر لجريان المائع و معادلتى عدم التوازن الحراري المحلي لتدفق الحرارة لوصف خصائص الجريان داخل الحيز المسامي. ان النتائج العددية تم الحصول عليها لمدى واسع من المتغيرات و هي نسبة عرض فتحة الدخول للحيز الى ارتفاع الحيز ($D/H = 0.1 - 0.6$) و المسامية لرغوة الالمنيوم ($\varepsilon = 0.91, 0.97$) و رقم كراشوف ($Gr = 10^4 - 3 \times 10^6$) و رقم رينولدز ($Re = 1 - 20$). ان تأثير الخواص الفيزيائية الوثيقة الصلة تم دراستها بدلالة مجالي الجريان و درجات الحرارة بالإضافة للتغير معدل قيم نسلت. لقد اظهرت النتائج المستحصلة ان معدل نسلت يزداد بزيادة D/H و Re و ينخفض بزيادة المسامية. ان الفرق بين توزيع درجة حرارة المائع و توزيع درجة حرارة الجزء الصلب قليل جدا.

الكلمات الرئيسية: الحمل المختلط, حيز مربع ذو فتحات, عدم التوازن الحراري, دراسة عددية, رغوة معدنية, وسط مسامي.



1. INTRODUCTION

The study of fluid flow and heat transfer induced by the combined effects of natural and forced convection, referred as mixed convection, in porous media is substantially increased in recent years due to its wide practical applications encountered in engineering and natural science. Some of these applications involve use of metal foams for enhanced cooling in electronic equipment, foam filled heat exchangers, open-cell metal foams, and solar energy collectors.

The pure conduction, natural convection, forced convection, and mixed convection of a lid driven square enclosure which is filled with water-saturated aluminum foams, and provided with a bottom heated wall and a top moving wall was investigated numerically by **Jeng, and Tzeng, 2008**. Their work uses the Brinkman-Forchheimer model for the momentum equation and the two-equation model for the energy equation. The variable parameters included the porosity of the aluminum foams, the Grashof number, and the Reynolds number. They found that the fluid temperature distribution differs little from the solid temperature distribution which means that one-equation model for energy may be employed to save computational time. Additionally, the higher porosity promotes much more enhancement of convective heat transfer while the lower porosity is important for higher total heat transfer due to the higher effective thermal conductivity value. **Kurtbas, and Celik, 2009** carried out an experimental study for the case of assisting mixed convection in a rectangular horizontal channel top and bottom heated surface and filled with aluminum foam of different pore densities. Different values of uniform heat flux, Reynolds number, Richardson number, and cross-sectional aspect ratio were tested and new empirical correlations had been constructed to link the Nusselt number. Later, **Venugopal, et al., 2010** developed a simple inexpensive metallic porous material and investigated experimentally the mixed convection heat transfer in a vertical duct with this metallic porous structure. It was showed that the developed porous medium has similar thermo-hydrodynamic performance to those seen in metal foams. The experimental study of hydraulic performance and heat transfer in flow assisted mixed convection in channel containing aluminum metal foams of high porosity was conducted by **Kamath, et al., 2011**. They utilized a wide range of Richardson and Reynolds numbers to cover the forced convection dominant and mixed convection regimes and developed useful heat transfer correlations.

Mixed convection flow in a lid-driven enclosure filled with a fluid-saturated porous medium was studied by many authors. **Khanafar, and Chamkha, 1999** investigated numerically the unsteady, laminar, mixed convection flow inside a square enclosure filled with a fluid-saturated uniform porous medium. The two vertical walls of the enclosure are insulated while the horizontal walls are maintained at constant temperatures with the top surface is moving from left to right at a constant speed. Furthermore, the enclosure filled with a fluid-saturated porous medium with top moving lid-driven wall and various types of boundary conditions was scrutinized numerically by number of authors like **Kumari, and Nath, 2011**, **Basak, et al., 2012**, **Oztop, et al., 2012**, and **Sivasankaran, and Pan, 2012**. The problem of mixed convection flow and heat transfer in a lid-driven cavity with heat generating porous medium was investigated numerically by **Muthamilselvan, et al., 2010**. The top and bottom walls are moving in opposite directions at different temperatures, while the side vertical walls are adiabatic. Moreover, laminar, two-dimensional, steady, mixed convection in a parallel two-sided lid-driven square cavity filled with a fluid-saturated porous medium was analyzed numerically by **Vishnuvardhanarao, and Das, 2008**. Then, a few number of articles considered the mixed convection flow and heat transfer in a two-sided lid-driven enclosures filled with fluid-saturated porous medium, such as **Kumar, et al., 2009**, **Vishnuvardhanarao, and Das, 2009**, and **Vishnuvardhanarao, and Das, 2010**.



The mixed convection can be resulted also from vented openings or exit ports. For this type of mixed convection **Mahmud, and Pop, 2006** studied numerically the steady mixed convection flow inside a square vented enclosure filled with a fluid-saturated porous medium. The vertical wall of the cavity is kept at constant temperature and the remaining walls are perfectly insulated. They assumed that the fluid and the porous medium are in local thermal equilibrium and the viscous drag and inertia terms of the momentum equations are negligible therefore they utilized the Darcy flow model in the momentum equation. The governing parameters performed in their work are the Rayleigh number, Peclet number, and the width of the inlet as a fraction of the height of the enclosure. **Ghazanfarian, and Abbassi, 2007** performed the steady laminar mixed convection inside a square cavity filled with a fluid-saturated porous medium and different positions of the outlet port. The same boundary conditions and flow model of **Mahmud, and Pop, 2006** was used and the governing equations had been solved by numerical finite difference method. While, **Barna, et al., 2008** constituted numerically the same vented enclosure and flow model in the momentum equation but with all enclosure walls being isothermal surfaces. Afterwards, **Rathish Kumar, and Krishna Murthy, 2010** proposed numerically the mathematical model for steady mixed convection process in a non-Darcian fluid saturated vertical enclosure under multiple Injection/Suction effects. To the best knowledge of the author, no attention has been paid to the problem of natural and mixed convection in vented enclosure filled with fluid-saturated metal foam. The present study focuses on a problem of steady natural and mixed convection inside a square vented cavity filled with water-saturated aluminum metal foam, with the left vertical sidewall being at constant temperature and the remaining enclosure walls being perfectly adiabatic. The Brinkman-Forchheimer-extended Darcy model in steady two dimensional and non-local thermal equilibrium are employed. The main objective of the present work is to investigate the influence of the flow governing parameters including Reynolds and Grashof numbers, and the width of the inlet and outlet as a fraction of the height of the enclosure for two types of aluminum metal foam on the flow characteristics. Numerical results are obtained for streamlines, isotherms for fluid and solid matrix, and the heat transfer rate at the heated wall in terms of local Nusselt number and average Nusselt number are presented graphically.

2. MATHEMATICAL FORMULATION

Consider a steady two-dimensional vented enclosure filled with a fluid saturated metal foam with the left vertical sidewall at constant temperature T_w whereas the other walls are well-insulated. The physical model of the problem is shown in **Fig. 1** which is a square enclosure of length H with a slot at the bottom edge of the vertical surface and a vent at the top edge for outflow. The slot and vent of width D are responsible of the forced convection arising while the buoyancy effects are induced because of the temperature difference of the left vertical sidewall and the stream temperature T_0 which has a constant velocity V_0 at the enclosure inlet. It is assumed that the porous medium is homogeneous, hydrodynamically and thermally isotropic and saturated with a fluid that is in thermal non-equilibrium with the solid matrix. The thermo-physical properties of the fluid and porous media are constant except for density dependency of the buoyancy term in the momentum equation, which is satisfied by the Boussinesq approximation. Under these assumptions, the conservation equations for mass, momentum and energy for the two-dimensional laminar thermal non-equilibrium model are, **Nield, and Bejan, 2006**:



$$\frac{\partial u}{\partial x} + \frac{\partial v}{\partial y} = 0 \quad (1)$$

$$\frac{1}{\varepsilon^2} \left(\rho_f u \frac{\partial u}{\partial x} + \rho_f v \frac{\partial u}{\partial y} \right) = -\frac{\partial p}{\partial x} + \frac{\mu_f}{\varepsilon} \left(\frac{\partial^2 u}{\partial x^2} + \frac{\partial^2 u}{\partial y^2} \right) - \frac{\mu_f}{K} u - \frac{C_F \rho_f}{K^{1/2}} \sqrt{u^2 + v^2} u \quad (2)$$

$$\frac{1}{\varepsilon^2} \left(\rho_f u \frac{\partial v}{\partial x} + \rho_f v \frac{\partial v}{\partial y} \right) = -\frac{\partial p}{\partial y} + \frac{\mu_f}{\varepsilon} \left(\frac{\partial^2 v}{\partial x^2} + \frac{\partial^2 v}{\partial y^2} \right) - \frac{\mu_f}{K} v - \frac{C_F \rho_f}{K^{1/2}} \sqrt{u^2 + v^2} v + \rho_f \beta g (T_f - T_0) \quad (3)$$

$$(\rho C_p)_f \left[u \frac{\partial T_f}{\partial x} + v \frac{\partial T_f}{\partial y} \right] = \left\{ \frac{\partial}{\partial x} [(k_f^* + k_d) \frac{\partial T_f}{\partial x}] + \frac{\partial}{\partial y} [(k_f^* + k_d) \frac{\partial T_f}{\partial y}] \right\} + h_v (T_s - T_f) \quad (4)$$

$$k_s^* \left[\frac{\partial^2 T_s}{\partial x^2} + \frac{\partial^2 T_s}{\partial y^2} \right] + h_v (T_f - T_s) = 0 \quad (5)$$

where k_f^* and k_s^* are given by **Calmidi, and Mahajan, 2000**:

$$k_f^* = \varepsilon k_f \quad (6)$$

$$k_s^* = 0.195(1 - \varepsilon)^{0.763} k_s \quad (7)$$

The hydrodynamic and thermal boundary conditions are specified as:

$$\text{Left isothermal wall: } u = v = 0, T_f = T_s = T_w \quad \text{on } x = 0, 0 \leq y \leq H \quad (8a)$$

$$\text{Inlet: } u = 0, v = V_0, T_f = T_s = T_0 \quad \text{on } y = 0, 0 \leq x \leq D \quad (8b)$$

$$\text{Bottom adiabatic wall: } u = v = 0, \frac{\partial T_f}{\partial y} = \frac{\partial T_s}{\partial y} = 0 \quad \text{on } y = 0, D \leq x \leq H \quad (8c)$$

$$\text{Right adiabatic wall: } u = v = 0, \frac{\partial T_f}{\partial y} = \frac{\partial T_s}{\partial y} = 0 \quad \text{on } x = H, 0 \leq y \leq H \quad (8d)$$

$$\text{Outlet: } u = 0, \frac{\partial T_f}{\partial y} = \frac{\partial T_s}{\partial y} = 0 \quad \text{on } y = H, 0 \leq x \leq D \quad (8e)$$

$$\text{Upper adiabatic wall: } u = v = 0, \frac{\partial T_f}{\partial y} = \frac{\partial T_s}{\partial y} = 0 \quad \text{on } y = H, D \leq x \leq H \quad (8f)$$

The following dimensionless parameters are utilized in the present study:

$$X = \frac{x}{H}, \quad Y = \frac{y}{H}, \quad U = \frac{u}{V_0} = \frac{\partial \psi}{\partial Y}, \quad V = \frac{v}{V_0} = -\frac{\partial \psi}{\partial X}, \quad P = \frac{p}{\rho_f V_0^2}, \quad Re = \frac{\rho_f V_0 H}{\mu_f}, \quad Da = \frac{K}{H^2}, \quad \theta_f = \frac{T_f - T_0}{T_w - T_0},$$

$$Gr = \frac{g \beta (T_w - T_0) \rho_f^2 H^3}{\mu_f^2}, \quad \theta_f = \frac{T_f - T_0}{T_w - T_0}, \quad \theta_s = \frac{T_s - T_0}{T_w - T_0}, \quad Pr = \frac{\mu_f C_f}{k_f}, \quad Nu_{fs} = \frac{h_v H^2}{k_f}, \quad \omega = -\frac{\partial U}{\partial Y} + \frac{\partial V}{\partial X} \quad (9)$$



Substitute these dimensionless variables into Eqs. (1)-(5) and (8), the corresponding dimensionless governing equations and boundary conditions are written as:

$$-\omega = \frac{\partial^2 \psi}{\partial X^2} + \frac{\partial^2 \psi}{\partial Y^2} \quad (10)$$

$$U \frac{\partial \omega}{\partial X} + V \frac{\partial \omega}{\partial Y} = -\frac{\varepsilon^2 \omega}{ReDa} + \frac{\varepsilon}{Re} \left(\frac{\partial^2 \omega}{\partial X^2} + \frac{\partial^2 \omega}{\partial Y^2} \right) - \frac{\varepsilon^2 C_F}{Da^{1/2}} \omega \sqrt{U^2 + V^2} - \frac{\varepsilon^2 C_F}{Da^{1/2}} \left(V \frac{\partial}{\partial X} (\sqrt{U^2 + V^2}) - U \frac{\partial}{\partial Y} (\sqrt{U^2 + V^2}) \right) + \frac{\varepsilon^2 Gr}{Re^2} \frac{\partial \theta_f}{\partial X} \quad (11)$$

$$U \frac{\partial \theta_f}{\partial X} + V \frac{\partial \theta_f}{\partial Y} = \frac{1}{RePr} \left\{ \frac{\partial}{\partial X} \left[\left(\frac{k_f^* + k_d}{k_f} \right) \frac{\partial \theta_f}{\partial X} \right] + \frac{\partial}{\partial Y} \left[\left(\frac{k_f^* + k_d}{k_f} \right) \frac{\partial \theta_f}{\partial Y} \right] \right\} + \frac{Nu_{fs}}{RePr} (\theta_s - \theta_f) \quad (12)$$

$$\frac{k_s^*}{k_f} \left[\frac{\partial^2 \theta_s}{\partial X^2} + \frac{\partial^2 \theta_s}{\partial Y^2} \right] + Nu_{fs} (\theta_f - \theta_s) = 0 \quad (13)$$

where k_d is the thermal dispersion and was obtained by the empirical equation modified by **Calmidi, and Mahajan, 2000**:

$$\frac{k_d}{k_f} = 0.06 Re Pr \sqrt{Da} \sqrt{U^2 + V^2} \quad (14)$$

h_v is the volumetric heat transfer of aluminum foam was also calculated by the empirical equation reported by **Calmidi, and Mahajan, 2000**:

$$\frac{h_v d^2}{k_f} = C_T \left(\frac{\rho_f \sqrt{U^2 + V^2} d}{\mu_f \varepsilon} \right)^{0.5} Pr^{0.37} \quad (15)$$

The dimensionless boundary conditions are casted as:

$$\text{Left isothermal wall: } U = V = 0, \psi = 0, \omega = -\frac{\partial^2 \psi}{\partial X^2}, \theta_f = \theta_s = 1 \quad \text{on } X = 0, 0 \leq Y \leq 1 \quad (16a)$$

$$\text{Inlet: } U = 0, V = 1, \psi = -X, \omega = -\frac{\partial^2 \psi}{\partial Y^2}, \theta_f = \theta_s = 0 \quad \text{on } Y = 0, 0 \leq X \leq D/H \quad (16b)$$

$$\text{Bottom adiabatic wall: } U = V = 0, \psi = -\frac{D}{H}, \omega = -\frac{\partial^2 \psi}{\partial Y^2}, \frac{\partial \theta_f}{\partial Y} = \frac{\partial \theta_s}{\partial Y} = 0 \quad \text{on } Y = 0, D/H \leq X \leq 1 \quad (16c)$$

$$\text{Right adiabatic wall: } U = V = 0, \psi = -\frac{D}{H}, \omega = -\frac{\partial^2 \psi}{\partial X^2}, \frac{\partial \theta_f}{\partial X} = \frac{\partial \theta_s}{\partial X} = 0 \quad \text{on } X = 1, 0 \leq Y \leq 1 \quad (16d)$$

$$\text{Outlet: } U = 0, \frac{\partial \psi}{\partial Y} = 0, \frac{\partial \theta_f}{\partial Y} = \frac{\partial \theta_s}{\partial Y} = 0 \quad \text{on } Y = 1, 0 \leq X \leq D/H \quad (16e)$$



Top adiabatic wall: $U = V = 0$, $\psi = -\frac{D}{H}$, $\omega = -\frac{\partial^2 \psi}{\partial Y^2}$, $\frac{\partial \theta_f}{\partial Y} = \frac{\partial \theta_s}{\partial Y} = 0$ on $Y = 1$, $D/H \leq X \leq 1$ (16f)

Equations (10) to (13) are solved numerically with the applied boundary conditions to simulate the mixed convection in the vented enclosure. The local Nusselt number (Nu) and average Nusselt number (\overline{Nu}) at the left vertical heated wall are formulated as:

$$Nu = -\frac{k_f^* \frac{\partial \theta_f}{\partial X}}{k_f} \Big|_{X=0} - \frac{k_s^* \frac{\partial \theta_s}{\partial X}}{k_f} \Big|_{X=0} \quad (17)$$

$$\overline{Nu} = \int_0^1 \left(-\frac{k_f^* \frac{\partial \theta_f}{\partial X}}{k_f} \Big|_{X=0} - \frac{k_s^* \frac{\partial \theta_s}{\partial X}}{k_f} \Big|_{X=0} \right) dY \quad (18)$$

In the present study, the aluminum foam is chosen as the porous medium saturated with water. The numerical data properties of the fluid and solid phase used in the present work are given in **Table 1**.

3. NUMERICAL TECHNIQUE AND CODE VALIDATION

The governing equations for dimensionless vorticity, stream-function, and solid and fluid energy equations together with the boundary conditions were solved numerically using the method of finite difference. The spatial derivatives of the governing equations are approximated by the central difference scheme, **Patanker, 1980**. The finite difference scheme reduces the continuum problem to a discrete problem prescribed by a system of algebraic equations written as tri-diagonal matrix and this matrix was solved by a line-by-line procedure of tri-diagonal matrix algorithm (TDMA), **Patanker, 1980**. For convergence criteria, the relative variations of the vorticity, stream-function, and solid-phase and fluid-phase temperatures was less than 10^{-5} between successive iterations. Finally, algorithms based on the Simpson,s rule is employed to perform the numerical integration of the average Nusselt number.

An in-house numerical computer code was developed for the solution of the problem considered. The computer program was built in MATLAB R2010a software and consists of a main program and a TDMA solver subroutine and a subroutine for working out the numerical integration by Simpson's rule. Additionally, the program lasts from eight to twenty three hours depending on the Reynolds number value. The flow chart of the built computer program is illustrated in **Fig. 2**.

A uniform grid in X and Y directions is used in the calculation domain and all numerical results were checked for the grid independence analysis to evaluate a more convenient grid size by monitoring the average Nusselt number on the heated wall. This was achieved by obtaining solutions with an increasing number of grid nodes in X and Y directions, until a point is reached where the solution is unchanged with a further increase in the number of nodes. Grid convergence was studied for the case of $Re = 10$, $Gr = 10^6$, and $\varepsilon = 0.97$ with grid sizes from 60×60 to 140×140 . The percentage error accomplished from the grid independence test between the grid 100×100 , 120×120 , and 140×140 and the asymptotic value were 2.88%, 2.3%, and 1.91%, respectively. Moreover, the size of the grid size was refined until the average Nusselt number did not change by more than 1.42%. However, the grid 120×120 was chosen for further numerical results because it is a good compromise between computational time and accuracy requirements.

To validate the accuracy of the developed computer code for the present simulation, the results of the present numerical code were tested and compared with the work of, **Jeng, and Tzeng, 2008** in a

mixed convection of a lid driven square enclosure filled with two types of water-saturated aluminum foams for Reynolds number of 20 and different values of Grashof number varies from 10^4 to 3×10^6 . The comparison of the average Nusselt number on the bottom heated wall shows excellent agreement between the present and the previous results as illustrated in **Table 2**. These effects provide credence to the accuracies of the present code and numerical method.

4. RESULTS AND DISCUSSION

The governing equations are solved for a wide range of Reynolds number, Grashof number, and the width of the inlet as a fraction of the height of the enclosure (D/H). Two aluminum foams with various porosities were utilized in the numerical simulations of the present work and the working fluid was chosen as water as listed in **Table 1**. For each type of aluminum foam, the Reynolds number is varied from 1 to 20, the Grashof number is varied from 10^4 to 3×10^6 , and the width of the inlet as a fraction of the height of the enclosure (D/H) variations is from 0.1 to 0.6. Additionally, the value of Darcy number was taken as $Da = 7.5 \times 10^{-5}$ for the 0.97-porosity sample and $Da = 5 \times 10^{-5}$ for the 0.91-porosity aluminum foam sample.

The streamlines corresponding to five different D/H values and three values of Grashof numbers for the case of $Re = 1$ are shown in **Fig. 3**. In this case, natural convection is the dominant heat transfer mode. By increasing the Grashof number, the buoyancy forces are strengthened, and consequently, the vorticity component near the inlet of the vented cavity is strengthened especially when $Gr = 10^6$ for $\varepsilon = 0.91$ and $\varepsilon = 0.97$. Therefore, in the case of $\varepsilon = 0.97$ and $Gr = 10^6$, the buoyancy force is much greater than the shear force and it dominates the flow field resulting in a stronger vortex as illustrated in **Fig. 3c**. Moreover, the streamlines of $\varepsilon = 0.91$ and $Gr = 10^4$ with different D/H possess no vortex generation because of the low Grashof number which induces a negligible buoyancy force in the present porous enclosure as shown in **Fig. 3a**. Finally, the rotating vortex strength is decreased with the increasing of inlet width to enclosure height fraction.

The mechanism of heat transfer inside the vented cavity consists of the combination effect of forced and natural convection. Therefore, when the Reynolds number is increased to a higher value of $Re = 20$ relative to the Grashof number values considered in the present study, the primary mode of heat transfer is the forced convection. As a result, the weak natural convection regime weakens the strength of vorticity in the present cavity and this causes the flow field to be regular, without any rotating vortices as depicted in **Fig. 4**. It also can be noticed that, the streamlines are the same for different Grashof number values at certain width of the inlet as a fraction of the height of the enclosure (D/H) value. Besides, the value of the streamline is decreased with the increasing of D/H value for specific value of Gr . This observation is noticed also from **Fig. 3** for the case of $Re = 1$.

Contours of fluid temperature for various ε and Gr values and $Re = 1$ and $Re = 20$ are presented in **Fig. 5** and **Fig. 6** respectively. From **Fig. 5a** and **Fig. 5b**, it can be observed that the increase in Grashof number for certain porosity value of $\varepsilon = 0.91$ has very little effect on the fluid isothermal lines compared with the increase of ε from 0.91 to 0.97 at $Gr = 10^6$. This is because the Grashof number promotes a stronger effect of buoyancy force with higher porosity than its increase influence at certain porosity value. As a result, the regions of higher temperature are constricted with the increasing of porosity. Also, it is regarded from **Fig. 5** that the increase in the inlet width to enclosure height fraction (D/H) increases the amount of natural convection which results in a wider regions of lower fluid temperature values. This is owing to the D/H increase that leads to higher amount of cold fluid enters the cavity compared with hot left vertical side temperature of the

enclosure which means higher natural convection quantity. As the Reynold number is increased to 20, the same behavior of the ε , Gr , and D/H variation is clearly shown in **Fig. 6** but with expanded lower temperature regions compared with the case of $Re = 1$. This is because of the stronger forced convection effect which tends to increase with the porosity and D/H increase and permits higher convection currents of lower inlet temperature to the enclosure compared with the hot wall temperature of the enclosure. **Fig. 6a** and **Fig. 6b** depicts the negligible effect of Grashof number for certain ε and D/H compared with the simultaneous monitoring of **Fig. 6b** and **Fig. 6c** of different porosity and certain Grashof number value of 10^6 . It is also clearly depicted that the fluid isothermal lines become nearly parallel to the hot wall left vertical side with the increasing of the D/H values especially when the porosity is 0.97, the Grashof number is 10^6 , the inlet width to enclosure height fraction is 0.5 and 0.6 as illustrated in **Fig. 6c**.

The isothermal lines of solid matrix is displayed for various porosity and Grashof number values and Reynolds number of 1 and 20 are displayed in **Fig. 7** and **Fig. 8** respectively. By comparing the isothermal lines depicted in **Fig. 5** and **Fig. 7** for $Re = 1$ and **Fig. 6** and **Fig. 8** for $Re = 20$, it is indicated that the fluid temperature distribution has a little difference from the solid matrix temperature distribution. Therefore, the thermal equilibrium energy equation model may be utilized for computational time saving with good accuracy.

The local Nusselt number distribution at the left vertical heated wall for different values of D/H , Reynolds number, and certain value of Grashof number value of 10^4 is demonstrated in **Fig. 9a** and **Fig. 9b** for $\varepsilon = 0.91$ and $\varepsilon = 0.97$ respectively. It is clear from these two figures that the Nusselt number decreases with increasing Y and Nu is high in magnitude at the lower left region of the enclosure. This is because of the higher values of temperature gradient around this region. Besides, the variation of the inlet width as a fraction of enclosure height and Reynolds number for the two types of aluminum metal foam have no considerable effect on the local Nusselt number values.

The average Nusselt number relation with the width of the inlet as a fraction of the enclosure height (D/H) at the left heated vertical sidewall for different Reynold and Grashof number values and the two porosities of aluminum foam is displayed in **Fig. 10**. The Nusselt number increases with the increasing of D/H and Re . That is, the temperature gradient of the fluid and solid matrix increases with D/H and Re . In such a situation the larger inlet will allow more forced flow which causes the fluid and solid matrix isotherms more concentrated to the left wall and tends to increase the temperature gradient and hence the average Nusselt number. Additionally, the increase of Reynolds number from 1 to 20 provides a much greater shear force effect than the buoyancy force effect and causes the fluid and solid matrix temperature gradient to increase as indicated previously in their temperature contours. This is also the reason behind the little influence of Grashof number increasing for certain ε value. Furthermore, the heat convection due to fluid flow is better in the higher-porosity aluminum foam. Accordingly, a lower average Nusselt number value is resulted because of the smaller value of the effective thermal conductivity and the decreasing of the temperature gradient of the fluid and solid matrix of the water saturated aluminum metal foam with the increasing of porosity, see **Fig. 10a** and **Fig. 10b**.

5. CONCLUSION

A numerical investigation of natural and mixed convection in a square vented enclosure filled with water saturated aluminum metal foam and heated at constant temperature on the left vertical side and the other walls are thermally insulated is demonstrated in the present paper. The variable



parameters included the Grashof number, the Reynolds number, the aluminum foam porosity, and the inlet width as a fraction of the enclosure height. The following conclusions are made from this scrutinization:

- The increasing of the Grashof number causes the vorticity component to strengthen near the cavity inlet and has no effect on the streamlines.
- The increasing of inlet width to enclosure height fraction and the Reynolds number tends to weaken the vorticity strength.
- The value of the streamline is decreased with the increasing of inlet width to enclosure height fraction value for specific value of Grashof number.
- The Grashof number increase for certain porosity value has very little effect on the fluid isothermal lines compared with the increase of porosity at specific Grashof number value which constrict higher temperature regions.
- Increasing the inlet width to enclosure height fraction results in a wider regions of lower fluid temperature values and these regions are more expanded with Reynolds number increasing.
- The fluid temperature distribution has a little difference from the solid matrix temperature distribution.
- The average Nusselt number increases with the increasing of inlet width to enclosure height fraction and Reynolds number and the porosity decreasing
- Grashof number variation has very little influence on the average Nusselt number values.

REFERENCES

- Barna, S. F., Bhuiyan, A. A., Banna, M. H., and Sadrul Islam, A. K. M., 2008, *Effect of Inlet to Cavity Width Ratio on Mixed Convection in a Microstructure Filled Vented Cavity*, Proceedings of the 4th BSME-ASME Int. Conf. on Thermal Engineering, Dhaka, Bangladesh, 27-29.
- Basak, T., Roy, S., and Chamkha, A. I., 2012, *A Peclet Number Based Analysis of Mixed Convection for Lid-Driven Porous Square Cavities with Various Heating of Bottom Wall*, Int. Comm. Heat and Mass Transfer, Vol. 39, PP. 657-664.
- Calmidi, V. V., and Mahajan, R. L., 2000, *Forced Convection in High Porosity Metal Foams*, ASME J. Heat Transfer, Vol. 122, PP. 557-565.
- Ghazanfarian, J., and Abbassi, A., 2007, *Mixed convection in a Square Cavity Filled with a Porous Medium and Different Exit Port Position*, J. Porous Media, Vol. 10, No. 7, PP. 701-718.
- Jeng, T., and Tzeng, S., 2008, *Heat Transfer in a Lid-Driven Enclosure Filled with Water-Saturated Aluminum Foams*, Numerical Heat Transfer, Part A, vol. 54, No. 2, PP. 178-196.
- Kamath, P. M., Balaaji, C., and Venkateshan, S. P., 2011, *Experimental Investigation of Flow Assisted Mixed Convection in High Porosity Foams in Vertical Channels*, Int. J. Heat and Mass Transfer, Vol. 54, PP. 5231-5241.



- Khanafer, K. M., and Chamkha, A. J., 1999, *Mixed Convection Flow in a Lid-Driven Enclosure Filled with a Fluid-Saturated Porous Medium*, Int. J. Heat and Mass Transfer, Vol. 42, PP. 2465-2481.
- Kurtbas, I., and Celik, N., 2009, *Experimental Investigation of Forced and Mixed Convection Heat Transfer in a Foam-Filled Horizontal Rectangular Channel*, Int. J. Heat and Mass Transfer, Vol. 52, PP. 1313-1325.
- Kumar, D. S., Dass, A. K., and Dewan, A., 2009, *Analysis of Non-Darcy Models for Mixed Convection in a Porous Cavity Using a Multigrid Approach*, Numerical Heat Transfer, Part A, Vol. 56, PP. 685-708.
- Kumari, M., and Nath, G., 2011, *Steady Mixed Convection Flow in a Lid-Driven Square Enclosure Filled with a Non-Darcy Fluid-Saturated Porous Medium with internal Heat Generation*, J. Porous Media, Vol. 14, No. 10, PP. 893-905.
- Mahmud, S., and Pop, I., 2006, *Mixed Convection in a Square Vented Enclosure Filled with a Porous Medium*, Int. J. Heat and Mass Transfer, Vol. 49, PP. 2190-2206.
- Muthamilselvan, M., Das, M. K., and Kandaswamy, P., 2010, *Convection in Lid-Driven Heat-Generating Porous Cavity with Alternative Thermal Boundary Conditions*, Transp. Porous Med., Vol. 82, PP. 337-346.
- Nield, D. A., and Bejan, A., 2006, *Convection in Porous Media*, 3rd Edition, Science Business Media, Inc. Springer, Berlin.
- Oztop, H. F., Varol, A., Pop, I., and Al-Saleem, K., 2012, *Mixed Convection in Partially Cooled Lid-Driven Cavity Filled with a Non-Darcy Porous Medium*, Progress in Computational Fluid Dynamics, Vol. 12, No. 1, PP. 46-55.
- Patanker, S. V., 1980, *Numerical Heat Transfer and Fluid Flow*, Hemisphere Publishing Corporation, United States of America.
- Rathish Kumar, B. V., and Krishna Murthy, S. V. S. N. V. G., 2010, *Mixed Convection in a Non-Darcian Fluid Saturated Square Porous Enclosure Under Multiple Suction Effect*, Int. J. Heat and Mass Transfer, Vol. 53, PP. 5764-5773.
- Sivasankaran, S., and Pan, K. L., 2012, *Numerical Simulation on Mixed Convection in a Porous Lid-Driven Cavity with Nonuniform Heating on Both Side Walls*, Numerical Heat Transfer, Part A, Vol. 61, PP. 101-121.
- Venugopal, G., Balaji, C., and Venkateshan, S. P., 2010, *Experimental Study of Mixed Convection Heat Transfer in a Vertical Duct Filled with Metallic Porous Structures*, Int. J. of Thermal Sciences, Vol. 49, PP. 340-348.



- Vishnuvardhanarao, E., and Das, M. K., 2008, *Laminar Mixed Convection in a Parallel Two-Sided Lid-Driven Differentially Heated Square Cavity Filled with a Fluid-Saturated Porous Medium*, Numerical Heat Transfer, Part A, Vol. 53, PP. 88-110.
- Vishnuvardhanarao, E., and Das, M. K., 2009, *Mixed Convection in a Buoyancy-Assisted Two-Sided Lid-Driven Cavity Filled with a Porous Medium*, Numerical Heat Transfer, Part A, Vol. 19, PP. 329-351.
- Vishnuvardhanarao, E., and Das, M. K., 2010, *Buoyancy Opposed Mixed Convection in a Two-Sided Lid-Driven Differentially Heated Square Cavity Filled with a Porous Medium*, J. Porous Media, Vol. 13, PP. 1059-1072.

NOMENCLATURE

C_F inertial coefficient of the porous medium.

C_{p_f} fluid specific heat at constant pressure, $J/kg \cdot ^\circ C$.

D width of the inlet and the vent, m .

g gravitational acceleration, m/s^2 .

h_v volumetric heat transfer coefficient, $W/m^3 \cdot ^\circ C$

H cavity height, m .

k_d thermal dispersion thermal conductivity, $W/m \cdot ^\circ C$.

k_f fluid thermal conductivity, $W/m \cdot ^\circ C$.

k_f^* effective fluid thermal conductivity, $W/m \cdot ^\circ C$.

k_s solid matrix thermal conductivity, $W/m \cdot ^\circ C$.

k_s^* effective solid matrix thermal conductivity, $W/m \cdot ^\circ C$.

K permeability of the porous medium, m^2 .

p effective pressure, Pa .

T_f fluid temperature, $^\circ C$.

T_0 temperature of the through flow at the inlet, $^\circ C$.

T_w temperature of the isothermal vertical surface, $^\circ C$.

T_s solid matrix temperature, $^\circ C$.

u velocity component along x –axis, m/s .

v velocity component along y –axis, m/s .

V_0 absolute value of the velocity of the forced flow at the inlet, m/s .

x, y Cartesian coordinates, m .

β coefficient of thermal expansion, $1/K$.

ε porosity.

μ_f fluid dynamic viscosity, $kg/m \cdot s$.

ρ_f fluid density, kg/m^3 .

ψ stream function.

ω vorticity.

Table 1. Properties of aluminum foams , **Jeng, and Tzeng, 2008** and **Calmidi, and Mahajan, 2000**, and saturated water.

	ε	PPI	$d(m)$	C_F	$K(\times 10^7 m^2)$	$k_s^* (W/m.K)$	$k_f^* (W/m.K)$	C_T
Al-foams	0.97	5	0.0005	0.097	2.7	2.928	0.595	0.108
	0.91	5	0.00055	0.085	1.8	6.77	0.558	0.332
Saturated water	$\rho_f(kg/m^3)$	$C_f(J/kg.K)$		$k_f(W/m.K)$			$\mu_f(Ns/m^2)$	
	997	4179		0.613			855×10^{-6}	

Table 2. Comparison of the average Nusselt number computed in the present work with the data reported by, **Jeng, and Tzeng, 2008** when $Re = 10$.

Porosity	Gr	Jeng, and Tzeng, 2008	Present study
$\varepsilon = 0.91$	10^4	11.954	11.8673
	3×10^6	24	24.9801
$\varepsilon = 0.97$	10^4	5.747	5.702
	10^6	12.5	12.4649

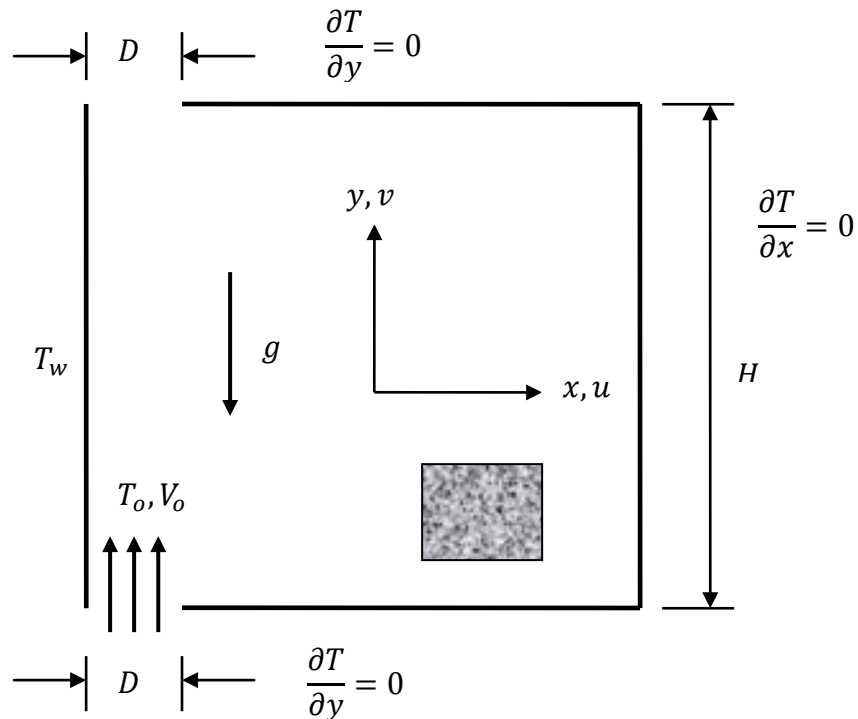


Figure 1. Physical model and the coordinate system of the cavity.

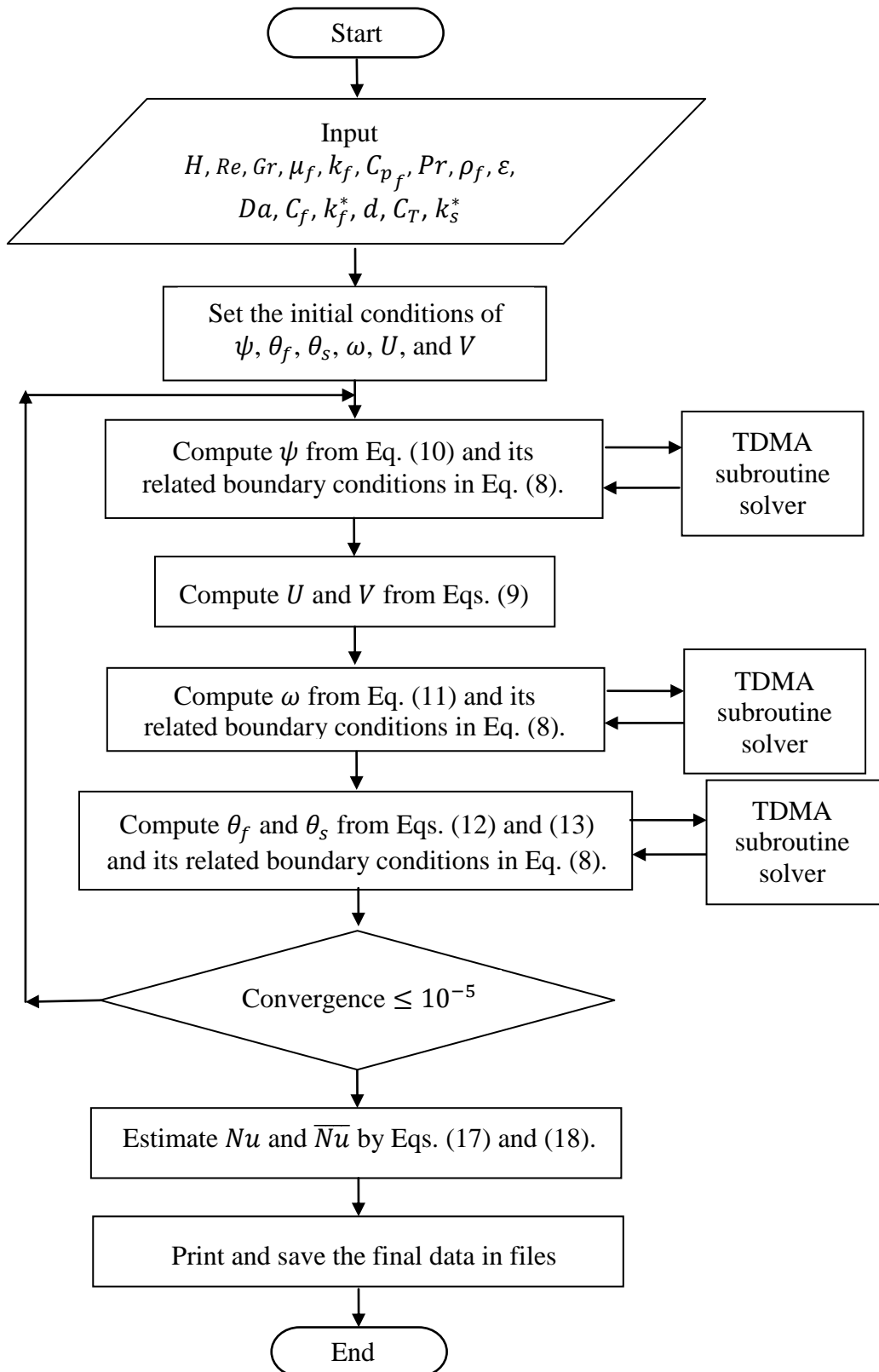


Figure 2. Flow Chart for the Computer Program.

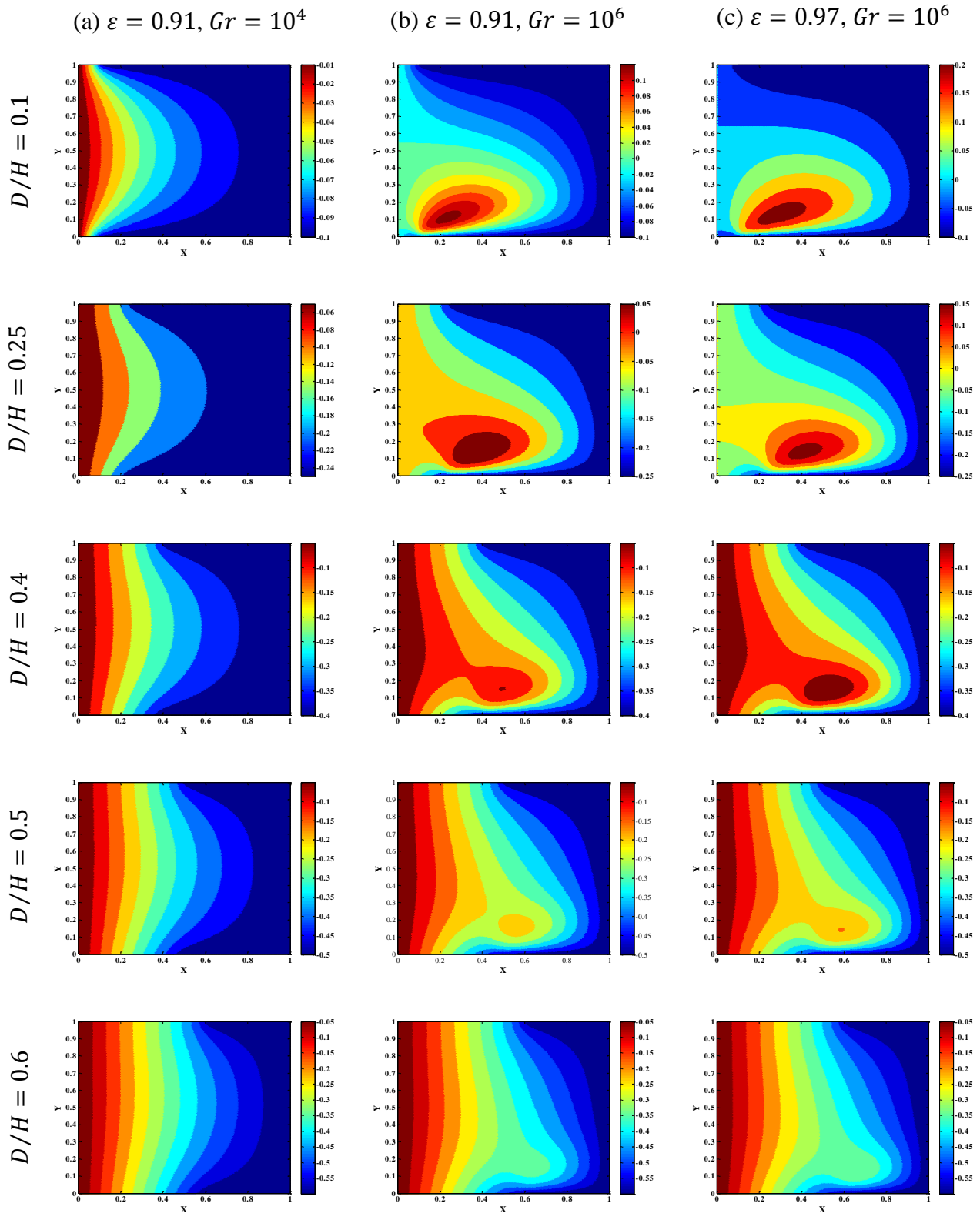


Figure 3. Streamlines for various ε, Gr , and D/H and $Re = 1$.

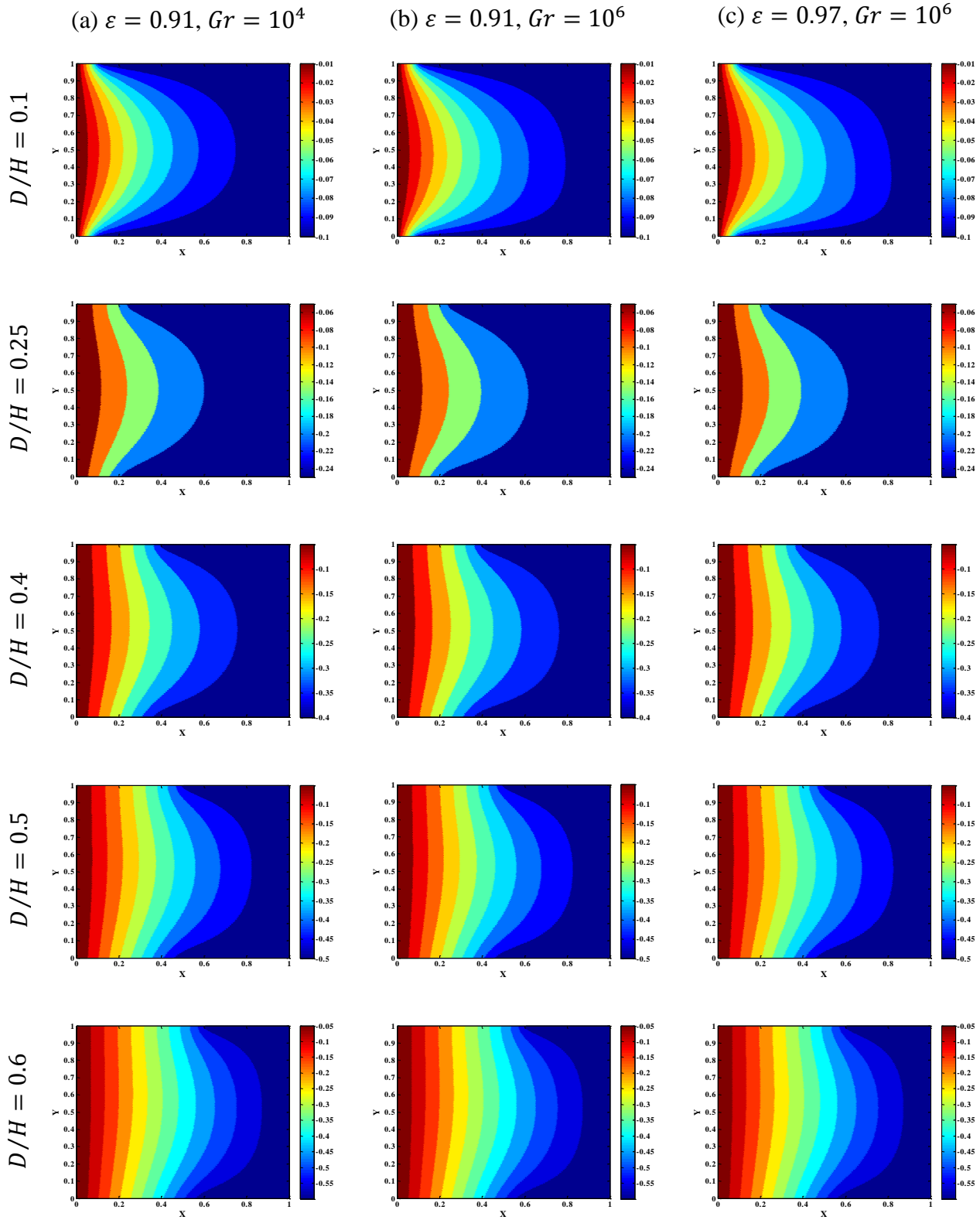


Figure 4. Streamlines for various ε , Gr , and D/H and $Re = 20$.

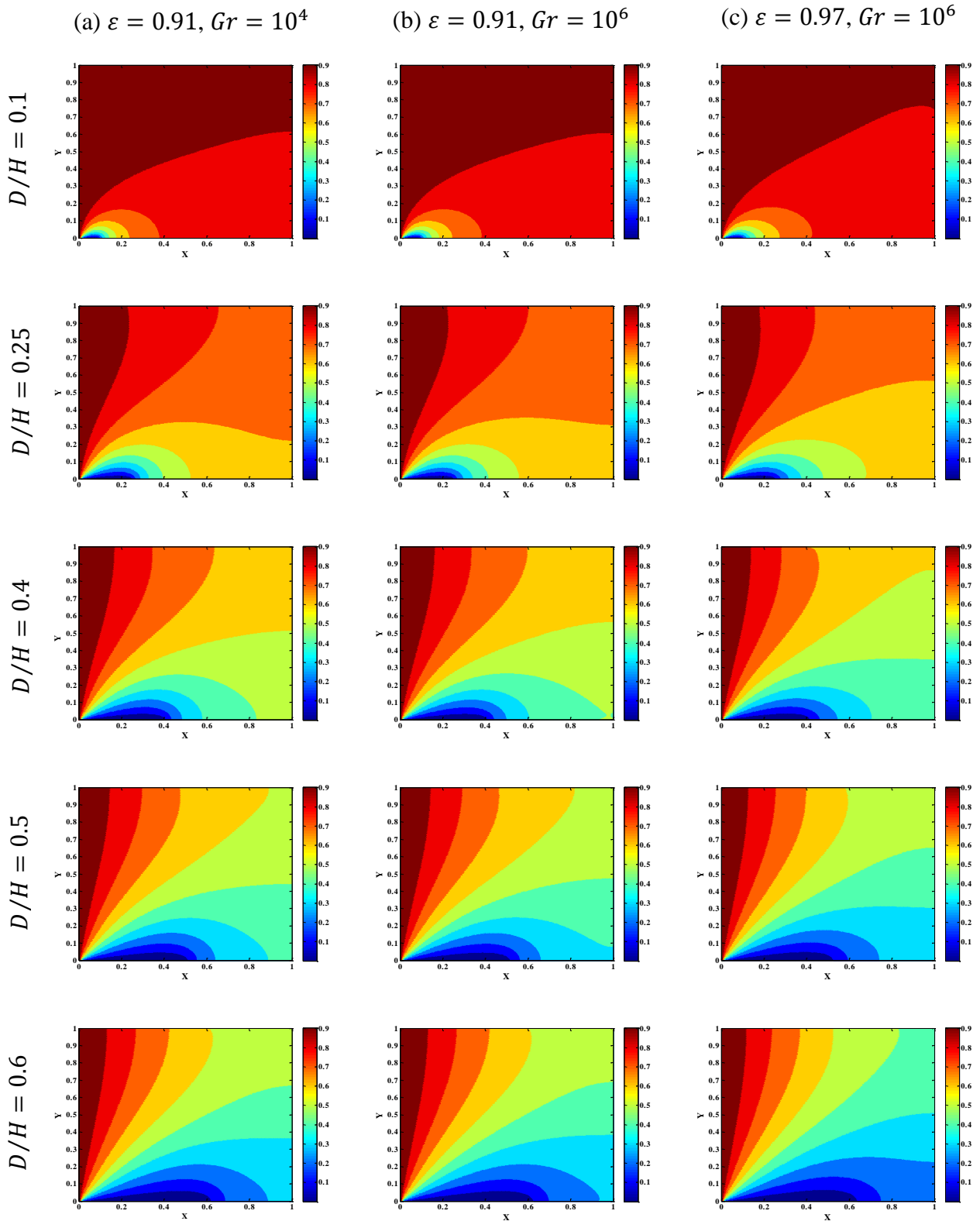


Figure 5. Isothermal lines of the fluid for various ε, Gr , and D/H and $Re = 1$.

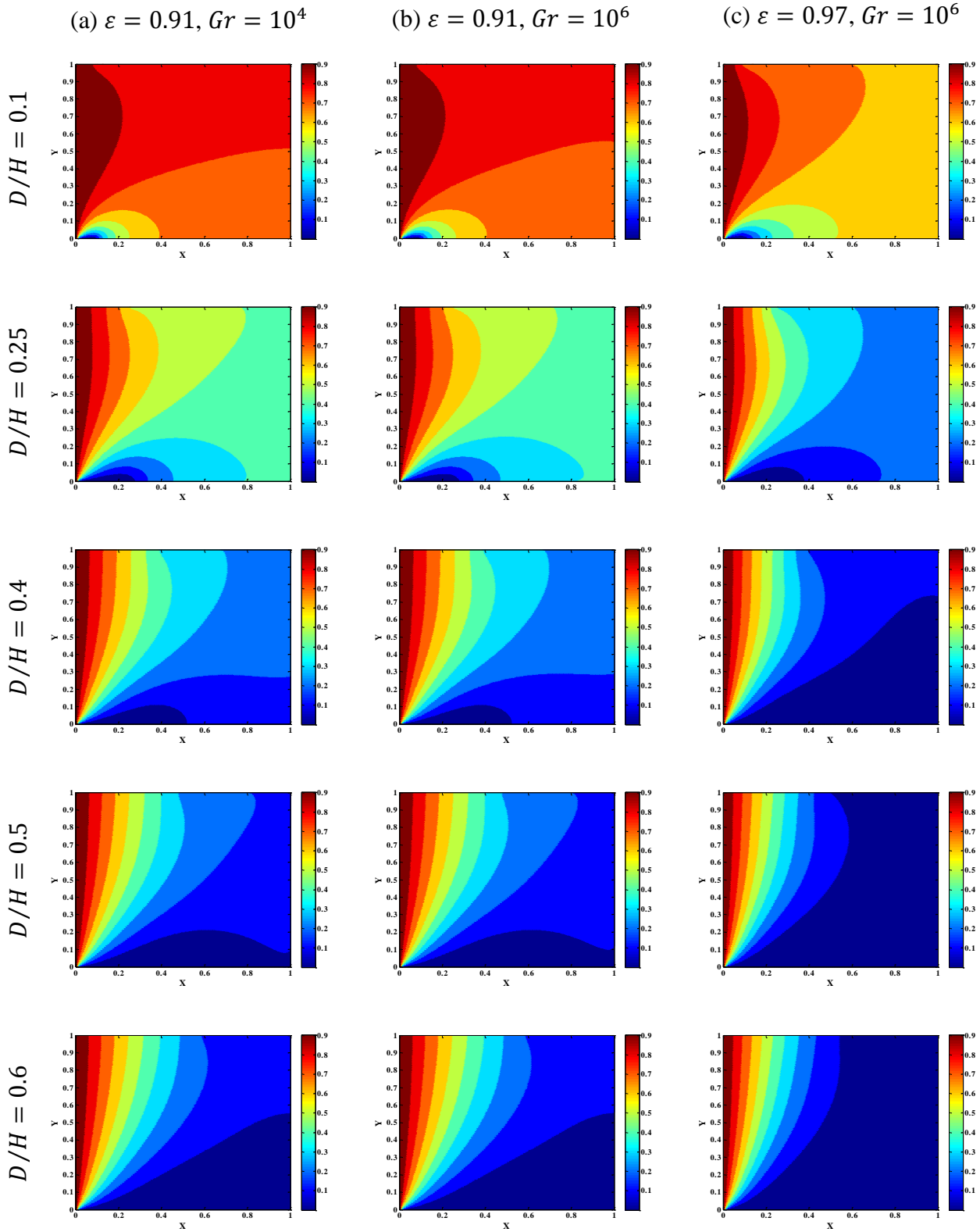


Figure 6. Isothermal lines of the fluid for various ε , Gr , and D/H and $Re = 20$.

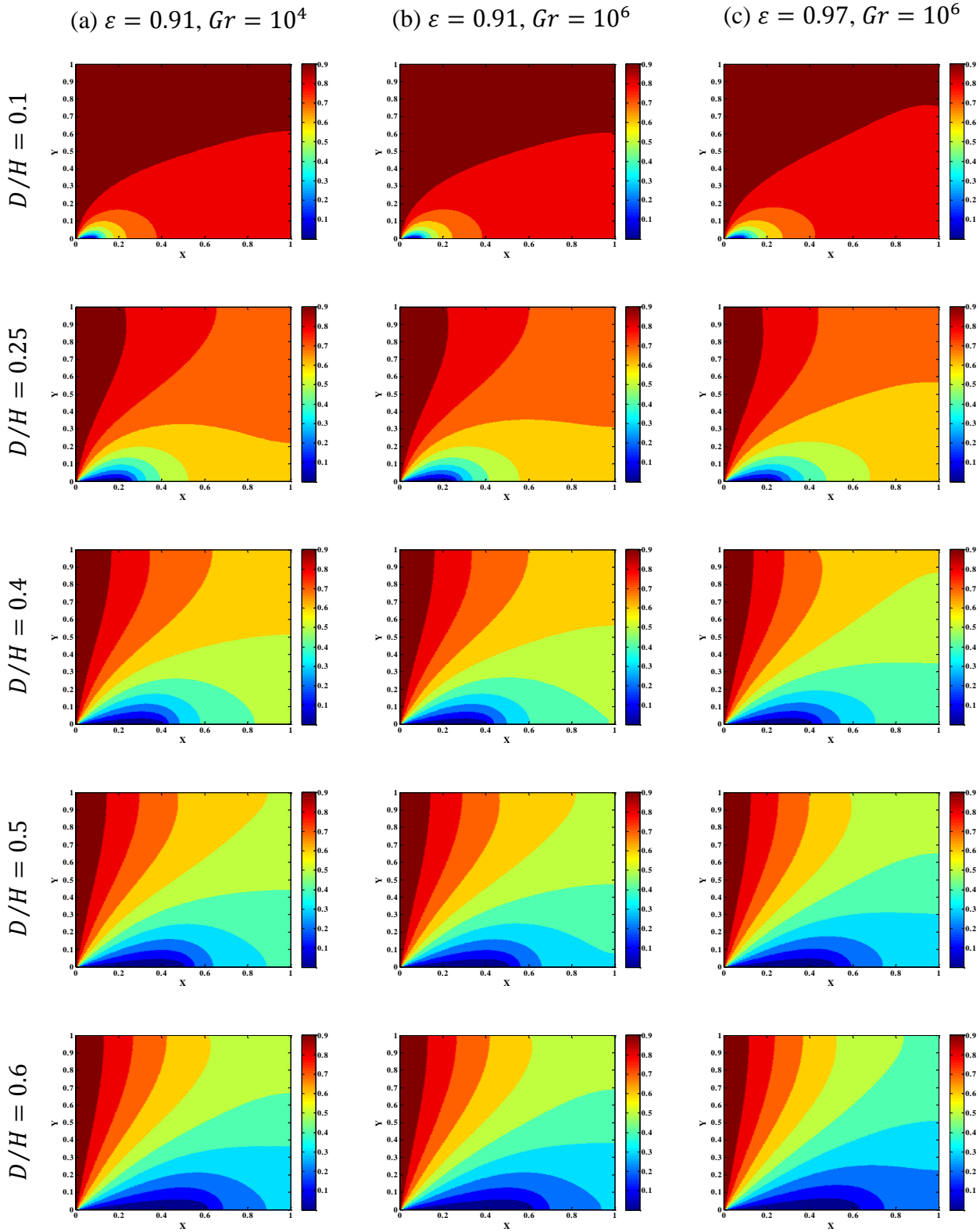


Figure 7. Isothermal lines of the solid matrix for various ε , Gr , and D/H and $Re = 1$.

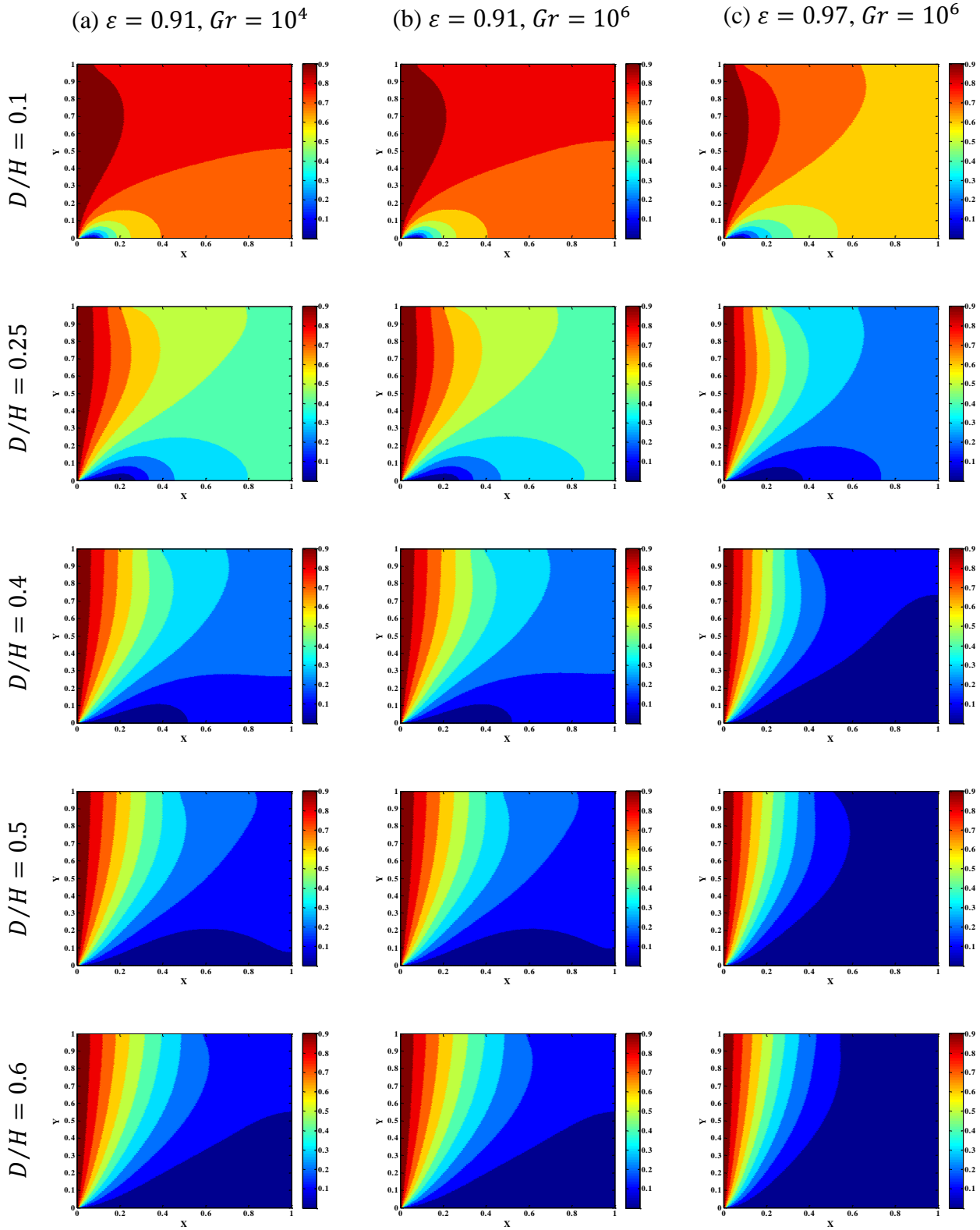


Figure 8. Isothermal lines of the solid matrix for various ε , Gr , and D/H and $Re = 20$.

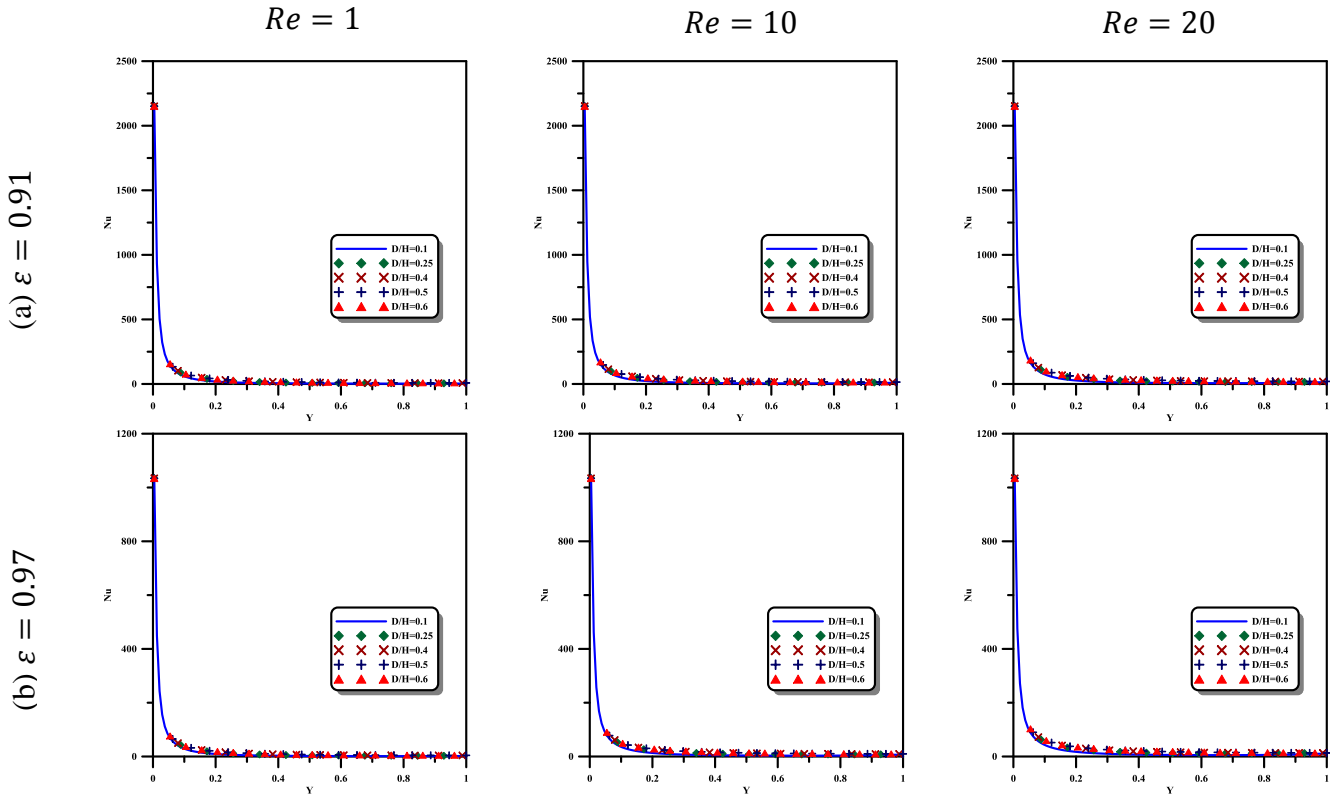


Figure 9. Local Nu as a function of D/H for various Re and $Gr = 10^4$.

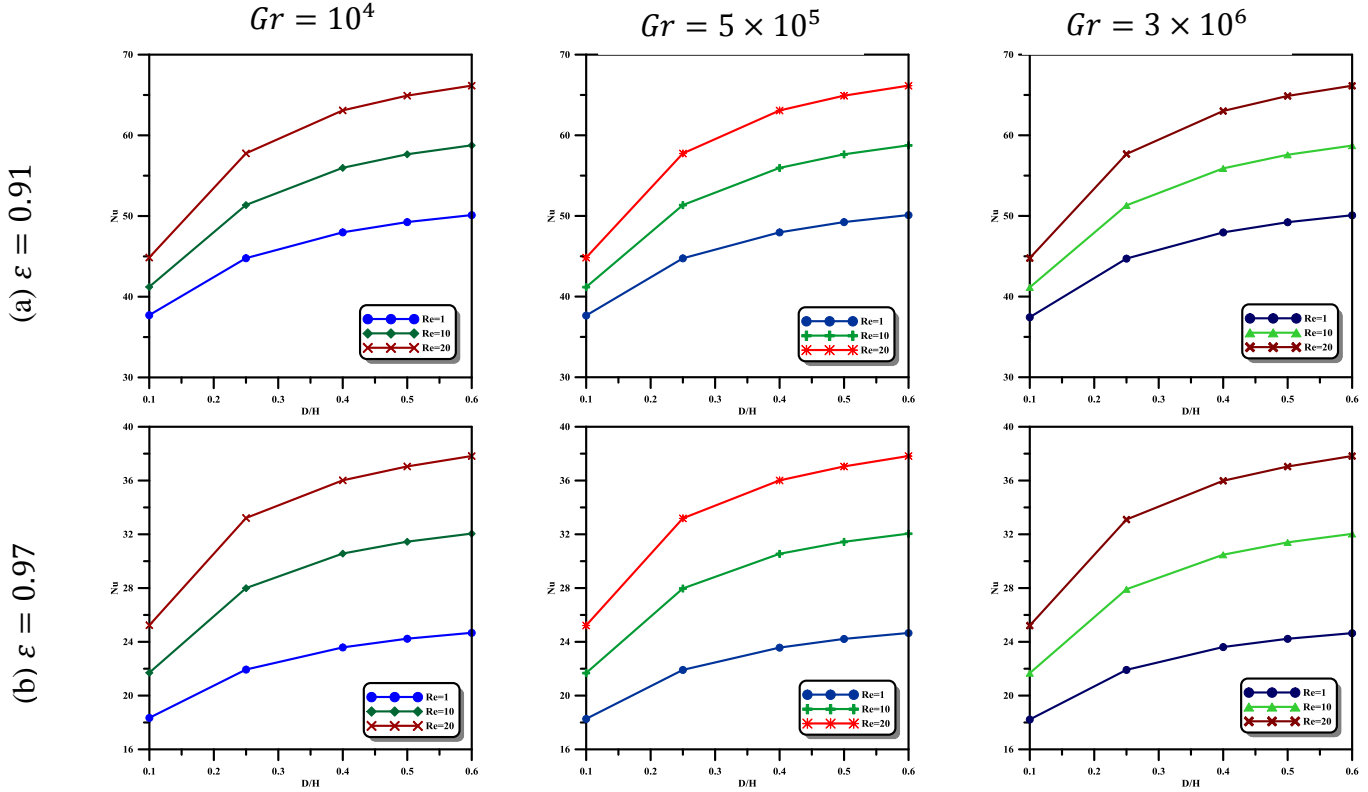


Figure 10. Average Nu as a function of D/H for various Re and Gr .